Geomechanics and Engineering, *Vol. 5, No. 6 (2013) 595-611*
DOI: http://dx.doi.org/10.12989/gae.2013.5.6.595

3D numerical model for wave-induced seabed response around breakwater heads

H.Y. Zhao [1], D.-S. Jeng [*1,2,3], Y. Zhang [2], J.-S. Zhang [3], H.J. Zhang [4] and C. Zhang [3]

[1] *Griffith School of Engineering, Griffith University Gold Coast Campus, Queensland, QLD 4222, Australia*
[2] *Center for Marine Geotechnical Engineering, Shanghai Jiao Tong University, Shanghai 200240, China*
[3] *State Key Laboratory of Hydrology-Water Resources and Hydraulic Engineering, Hohai University, Nanjing, 210098, China*
[4] *Faculty of Civil Engineering and Mechanics, Jiangsu University, Zhenjiang 212013, Jiangsu, China*

(*Received January 03, 2013, Revised July 22, 2013, Accepted August 06, 2013*)

Abstract. This paper presents a three-dimensional (3D) integrated numerical model where the wave-induced pore pressures in a porous seabed around breakwater heads were investigated. Unlike previous research, the Navier-Stokes equation is solved with internal wave generation for the flow model, while Biot's dynamic seabed behaviour is considered in the seabed model. With the present model, a parametric study was conducted to examine the effects of wave and soil characteristics and breakwater configuration on the wave-induced pore pressure around breakwater heads. Based on numerical examples, it was found that the wave-induced pore pressures at breakwater heads are greater than that beneath a breakwater. The wave-induced seabed response around breakwater heads become more important with: (i) a longer wave period; (ii) a seabed with higher permeability and degree of saturation; and (iii) larger angle between the incident waves and breakwater. Furthermore, the relative difference of wave-induced pore pressure between fully-dynamic and quasi-static solutions are larger at breakwater heads than that beneath a breakwater.

Keywords: breakwater; seabed response; wave-seabed-structure interactions; Biot's poro-elastic "quasi-static" and "fully-dynamic" model; Navier-Stokes equations

1. Introduction

Breakwaters are commonly constructed to reduce or eliminate the detrimental effects of wave forces on beaches, bluffs, dunes or harbour regions. When waves approach, the accompanying wave energy drives sediments to drift along the coast, resulting in erosion. The installation of breakwaters is an effective way to reduce erosion by forming an area of slack water behind the breakwater. Deposition occurs in this area and the beach is built up. On the other hand, the areas in front of the structure tend to shrink. In practice, breakwaters are seldom built for mere maintenance of a coastline's natural features, but are more often built for engineering purposes due to the high investment costs and possible renovation needs. Numerous failure mechanisms for the damage of marine structures were reported in the literature that, in particularly seabed foundation, such as sliding, overturning, bearing capacity failure, instantaneous liquefaction and liquefaction due to

*Corresponding author, Professor, E-mail: d.jeng@griffith.edu.au

http://www.techno-press.org/?journal=gae&subpage=7 ISSN: 2005-307X (Print), 2092-6219 (Online)

progressive buildup of pore pressure and excessive deformation. Furthermore, the interaction of the wave components complicates the soil response in the vicinity of breakwaters. In the past, damage has been observed in numerous marine structures due to seabed instability around these structures (Smith and Gordon 1983). Deep scours were also reported at the toes of marine structures (Gökee *et al*. 1994, Sumer and Fredsøe 2002).

By adopting the Biot's consolidation equation, Mase *et al*. (1994) developed a FEM numerical model to investigate the wave-induced pore water pressures and effective stress in a rubble mound breakwater under linear wave loading, in which the lateral boundary conditions are provided by the analytical solution proposed by Yamamoto (1977). Jeng *et al*. (2000) investigated the wave-induced pore pressure around a composite breakwater under linear standing wave using a FEM numerical model. Based on the modified Navier-Stokes equations and Biot's equations, Norimi *et al.* (1998) proposed a combined BEM-FEM model to record the dynamic soil response around the breakwater and the pore water pressure inside the breakwater. Another FEM numerical model, in which the fully dynamic 'u-w' form is taken as the governing equation is developed by Ulker *et al*. (2010) to investigate the dynamic response and instability of the seabed around a caisson breakwater.

All aforementioned studies for the wave-seabed-breakwater interactions have been limited to 2D cases. Only a few researches for 3D have been reported in the literature (Jeng 2003), but they only discussed the interaction in front of the breakwater. Li and Jeng (2008) and Jeng and Ou (2010) investigated the wave-induced soil response around breakwater heads with the poro-elastic and poro-elastoplastic seabed models. However, in their models, the breakwater is simplified as a single line without width and weight and only linear wave theory was considered.

In this paper, a new 3D model was proposed by integrating both wave and seabed models. In the wave model, water waves were generated by numerical internal wave-maker, taking the turbulence intensity into consideration; the wave pressure around the breakwater head can then be correctly evaluated. In a seabed, the wave-induced dynamic soil responses around the breakwater head were modeled by Biot's theory within COMSOL environment and the coupling between water wave and seabed was through data interface exchange. With the present model, a parametric study was conducted to examine the effects of wave and seabed characteristics and the configuration of breakwaters on the soil response in a porous seabed around breakwater heads.

2. Theoretical formulations

2.1 Wave model

The flow motion of incompressible fluid based on the classical Navier-Stokes equations derived from Newton's second law can be expressed as

$$\nabla \cdot u_f = 0 \tag{1}$$

$$\frac{\partial(\rho_f u_f)}{\partial t} + u_f \cdot \nabla(\rho_f u_f) = -\nabla p + \nabla \cdot \tau_f + \rho_f g \tag{2}$$

where u_f is the velocity field vector, p_f is the pressure, g is the gravity vector, t is the time, ρ_f is the density, τ_f is the shear stress tensor which can be defined as

$$\tau_f = \mu_f(\nabla u_f + \nabla^T u_f) \tag{3}$$

in which μ_f is the molecular viscosity.

The filtered continuity and momentum equations, Reynolds-Averaged Navier-Stokes, (RANS) can be obtained by applying the filter operation to Navier-Stokes equations (Eqs. (1) and (2)).

$$\frac{\partial \overline{u}_{fi}}{\partial x_i} = 0 \tag{4}$$

$$\frac{\partial\left(\rho_f \overline{u}_{fi}\right)}{\partial t} + \frac{\partial\left(\rho_f \overline{u_{fi}u_{fj}}\right)}{\partial x_i} = \frac{\partial \overline{p}_f}{\partial x_i} + \rho_f g_i + \frac{\partial}{\partial x_i}\left[\mu_f\left(\frac{\partial \overline{u}_{fi}}{\partial x_j} + \frac{\partial \overline{u}_{fj}}{\partial x_j}\right)\right] \tag{5}$$

where the overbar denotes the filtered variables, the unknown quantity $\overline{u_{fi}u_{fj}}$ in the filtering momentum equation can be defined as

$$\rho_f \overline{u_{fi}u_{fj}} = -\rho\mu_{ft}\left(\frac{\partial \overline{u}_{fi}}{\partial x_j} + \frac{\partial \overline{u}_{fj}}{\partial x_i}\right) + \frac{2}{3}k_r\delta_{ij} + \rho_f \overline{u}_{fi}\overline{u}_{fj} \tag{6}$$

where μ_{ft} and k_r are the turbulent viscosity and residual kinetic energy, respectively (Rodi 1980), and δ_{ij} is the Kronecker delta.

Based on Eq. (6), Eq. (5) can be expressed as

$$\frac{\partial\left(\rho_f \overline{u}_{fi}\right)}{\partial t} + \frac{\partial\left(\rho_f \overline{u}_{fi}\overline{u}_{fj}\right)}{\partial x_i} = -\frac{\partial \overline{p}_f}{\partial x_i} + \rho_f g_i + \frac{\partial}{\partial x_i}\left[\mu_{eff}\left(\frac{\partial \overline{u}_{fi}}{\partial x_j} + \frac{\partial \overline{u}_{fj}}{\partial x_j}\right)\right] \tag{7}$$

in which $\overline{p}_f$ is the modified filtered pressure, $\mu_{eff} = \mu_f + \mu_{ft}$ is the total effective viscosity.

The internal wave-maker method is used in the present study (Lin and Liu 1999). In the source region, a source function $S(x_i, t)$ is added into the mass conservation, Eq. (4), i.e.

$$\frac{\partial \overline{u}_{fi}}{\partial x_j} = S(x_i, t) \tag{8}$$

where $S(x_i, t) \neq 0$ within the source region, the value of $S(x_i, t)$ depends on wave characteristic.

2.2 Seabed model

Based on the Biot (1941, 1956) equations for saturated porous medium with compressible fluid and incompressible soil particles for dynamic problems, in which the effects of inertia terms of solid and fluid are taken into consideration, the governing equations are summarized in tensor form as below

$$\sigma_{ij,j} - \rho\ddot{u}_{si} - \rho_f \ddot{\overline{w}}_{fi} = 0 \tag{9}$$

$$(p_s)_{,i} - \rho_f \ddot{u}_{si} - \frac{\rho_f}{n}\ddot{\overline{w}}_{ft} - \frac{\rho_f g}{k_{ij}}\dot{\overline{w}}_{fj} = 0 \tag{10}$$

$$\dot{u}_{si,i} + \dot{\overline{w}}_{fi,i} + \frac{n}{K_f}\dot{p}_s = 0 \tag{11}$$

where σ_{ij} is the total stresses; u_{si} and w_{fi} are the displacement of soil and the relative displacement of fluid to soil, respectively; $\rho = (1-n)\rho_s + n\rho_f$ is the average density of the porous medium; ρ_f and ρ_s are the density of the solid and fluid, respectively; and ρ_s, n and k are the pore pressure, porosity and permeability coefficient, respectively.

In Eq. (11), K_f is the bulk modulus of the pore fluid, which can be defined as

$$\frac{1}{K_f} = \frac{1}{K_p} + \frac{1-S}{p_0} \tag{12}$$

where K_p is the bulk modulus of the fluid, which can be defined as 2×10^9 N/m^2, p_0 is the absolute pore pressure and S is the degree of saturation.

A new field variable can be used in the full-dynamic formulation, which can be defined as

$$U_{fi} = u_{si} + w_{fi} = u_{si} + \frac{\overline{w}_{fi}}{n} \tag{13}$$

where U is the total fluid displacement (Zienkiewicz and Shiomi 1984). Then Eqs. (9)-(11) can be rewritten in terms of U_f and u_s as

$$\sigma_{ij,j} - \rho\ddot{u}_{si} - \rho_f n\left(\ddot{U}_{fi} - \ddot{u}_{si}\right) = 0 \tag{14}$$

$$(p_s)_{,i} - \rho_f \ddot{u}_{si} - \rho_f\left(\ddot{U}_{fi} - \ddot{u}_{si}\right) - \frac{n\left(\ddot{U}_{fi} - \ddot{u}_{si}\right)}{k_{ij}}\rho_f g = 0 \tag{15}$$

$$\dot{u}_{si,i} + n\left(\ddot{U}_{fi} - \ddot{u}_{si}\right) + \frac{n}{K_f}\dot{p}_s = 0 \tag{16}$$

The relationship between the effective stress and the pore pressure on the saturated medium can be expressed as

$$\sigma_{ij,j} = \sigma'_{ij} - \delta_{ij} p_s \tag{17}$$

$$\sigma'_{ij,j} = \delta_{ij}(p_s) + \rho\ddot{u}_{si} + \rho_f n\left(\ddot{U}_{fi} - \ddot{u}_{si}\right) \tag{18}$$

The seabed is considered as isotropic, so the permeability (k) is the same in all directions. The pore pressure in Eq. (16) can be obtained as

$$p_s = -Q\left(u_{si,i}(1-n) + nU_{fi,i}\right) \tag{19}$$

The stress-strain relationship can be expressed as Hooke's law

$$\sigma'_{ij,j} = \lambda u_{si,i}\delta_{ij} + 2Gu_{si,i} \tag{20}$$

where G is shear modulus, μ_s is Poisson's ratio, $\lambda = 2G\mu_s / (1 - 2\mu_s)$ is the Lame's constant.

Substituting Eq. (15) into Eq. (14), together with Eqs. (19) and (20), the governing equations can be written in the scalar form as

$$\begin{aligned} &G\nabla^2 u_s + \frac{G}{(1-2\mu_s)}\frac{\partial \varepsilon_s}{\partial x} + (n-1)\rho_s \frac{\partial^2 u_s}{\partial t^2} - \frac{n^2 \rho_f g}{k_z}\frac{\partial u_s}{\partial t} \\ &= -(n-1)^2 Q\left(\frac{\partial^2 u_s}{\partial x^2} + \frac{\partial^2 u_s}{\partial x \partial y} + \frac{\partial^2 w_s}{\partial x \partial z}\right) + n(n-1)Q\left(\frac{\partial^2 U_f}{\partial x^2} + \frac{\partial^2 V_f}{\partial x \partial y} + \frac{\partial^2 W_f}{\partial x \partial z}\right) - \frac{n^2 \rho_f g}{k_z}\frac{\partial U_f}{\partial t} \end{aligned} \tag{21}$$

$$\begin{aligned} &G\nabla^2 v_s + \frac{G}{(1-2\mu_s)}\frac{\partial \varepsilon_s}{\partial y} + (n-1)\rho_s \frac{\partial^2 u_s}{\partial t^2} - \frac{n^2 \rho_f g}{k_z}\frac{\partial v_s}{\partial t} \\ &= -(n-1)^2 Q\left(\frac{\partial^2 u_s}{\partial x \partial y} + \frac{\partial^2 v_s}{\partial y^2} + \frac{\partial^2 w_s}{\partial y \partial z}\right) + n(n-1)Q\left(\frac{\partial^2 U_f}{\partial x \partial y} + \frac{\partial^2 V_f}{\partial y^2} + \frac{\partial^2 W_f}{\partial y \partial z}\right) - \frac{n^2 \rho_f g}{k_z}\frac{\partial V_f}{\partial t} \end{aligned} \tag{22}$$

$$\begin{aligned} &G\nabla^2 w_s + \frac{G}{(1-2\mu_s)}\frac{\partial \varepsilon_s}{\partial z} + (n-1)\rho_s \frac{\partial^2 w_s}{\partial t^2} - \frac{n^2 \rho_f g}{k_z}\frac{\partial w_s}{\partial t} \\ &= -(n-1)^2 Q\left(\frac{\partial^2 u_s}{\partial x \partial z} + \frac{\partial^2 v_s}{\partial y \partial z} + \frac{\partial^2 w_s}{\partial z^2}\right) + n(n-1)Q\left(\frac{\partial^2 U_f}{\partial x \partial z} + \frac{\partial^2 V_f}{\partial y \partial z} + \frac{\partial^2 W_f}{\partial z^2}\right) - \frac{n^2 \rho_f g}{k_z}\frac{\partial W_f}{\partial t} \end{aligned} \tag{23}$$

In which $Q = K_f / n$; ∇ is the Laplace operator; u_s, v_s, w_s are the soil displacement on the x-, y-, and z directions, respectively; U_f, V_f, W_f are the total fluid displacement on the x-, y-, z- direction, respectively; $\varepsilon_s = \frac{\partial u_s}{\partial x} + \frac{\partial v_s}{\partial y} + \frac{\partial w_s}{\partial z}$ is the volume strain.

Substituting Eq. (16) into Eq. (15), the equation of the pore fluid equilibrium can be expressed as

$$\begin{aligned} &n^2 Q\left(\frac{\partial^2 U_f}{\partial x^2} + \frac{\partial^2 V_f}{\partial x \partial y} + \frac{\partial^2 W_f}{\partial x \partial z}\right) - n\rho_f \frac{\partial^2 U_f}{\partial t^2} - \frac{n^2 \rho_f g}{k_z}\frac{\partial U_f}{\partial t} \\ &= n(n-1)Q\left(\frac{\partial^2 u_s}{\partial x^2} + \frac{\partial^2 v_s}{\partial x \partial y} + \frac{\partial^2 w_s}{\partial x \partial z}\right) - \frac{n^2 \rho_f g}{k_z}\frac{\partial u_s}{\partial t} \end{aligned} \tag{24}$$

$$\begin{aligned} &n^2 Q\left(\frac{\partial^2 U_f}{\partial x \partial y} + \frac{\partial^2 V_f}{\partial y^2} + \frac{\partial^2 W_f}{\partial y \partial z}\right) - n\rho_f \frac{\partial^2 U_f}{\partial t^2} - \frac{n^2 \rho_f g}{k_z}\frac{\partial V_f}{\partial t} \\ &= n(n-1)Q\left(\frac{\partial^2 u_s}{\partial x \partial y} + \frac{\partial^2 v_s}{\partial y^2} + \frac{\partial^2 w_s}{\partial y \partial z}\right) - \frac{n^2 \rho_f g}{k_z}\frac{\partial v_s}{\partial t} \end{aligned} \tag{25}$$

$$n^2Q\left(\frac{\partial^2 U_f}{\partial x\partial z}+\frac{\partial^2 V_f}{\partial y\partial z}+\frac{\partial^2 W_f}{\partial z^2}\right)-n\rho_f\frac{\partial^2 W_f}{\partial t^2}-\frac{n^2\rho_f g}{k_z}\frac{\partial W_f}{\partial t}$$
$$=n(n-1)Q\left(\frac{\partial^2 u_s}{\partial x\partial z}+\frac{\partial^2 v_s}{\partial y\partial z}+\frac{\partial^2 w_s}{\partial z^2}\right)-\frac{n^2\rho_f g}{k_z}\frac{\partial w_s}{\partial t} \tag{26}$$

For a simplified case, the quasi-static consolidation problems, all the inertia terms are ignored, after substituting Eq. (11) into (10), the governing equations become

$$\sigma_{ij,j}=0 \tag{27}$$

$$\dot{\varepsilon}_{sii}+\left(\frac{k_{ij}}{\gamma_w}(p_{s,j})\right)+\frac{n}{K_f}\dot{p}_s=0 \tag{28}$$

Substituting Eq. (19) into Eq. (28) the governing equations can be rewritten as

$$G\nabla^2 u_s+\frac{G}{(1-2\mu_s)}\frac{\partial\varepsilon_s}{\partial x}=\frac{\partial p_s}{\partial x} \tag{29}$$

$$G\nabla^2 v_s+\frac{G}{(1-2\mu_s)}\frac{\partial\varepsilon_s}{\partial y}=\frac{\partial p_s}{\partial y} \tag{30}$$

$$G\nabla^2 w_s+\frac{G}{(1-2\mu_s)}\frac{\partial\varepsilon_s}{\partial z}=\frac{\partial p_s}{\partial z} \tag{31}$$

$$\nabla^2 p_s-\frac{\gamma_w n\beta}{k_z}\frac{\partial p_s}{\partial t}=\frac{\gamma_w}{k_z}\frac{\partial\varepsilon_s}{\partial t} \tag{32}$$

Where ε_s is the volumetric strain. $B = 1 / K_f$ is the compressibility of the pore fluid. If non-ho mogenous seabed such as variable permeability is considered, the previous framework for analytical solutions (Jeng and Seymour 1997) can be adopted.

2.3 Boundary conditions

To solve the wave field, appropriate boundary conditions are required. For the turbulence field, the log-law distribution of mean tangential velocity in the turbulent boundary layer is imposed near the rigid boundary. Both the turbulent kinetic energy and its dissipation rate on the free surface are implemented with zero–gradient boundary conditions. The damping zones located at two vertical boundaries which are far from the concerned region are applied for velocity component in order to avoid the reflection of waves and interference of on current inlet/outlet. To obtain computational stability, the time interval is automatically adjusted at each time step to satisfy Cournat-Friedrichs-Lewy condition and the diffusive limit condition (Lin and Liu 1999).

For a porous seabed, appropriate boundary conditions are also required for the evaluation of the

wave-induced seabed response. First, the wave-induced effective stress and shear stress is negligible at the seabed surface ($z = 0$) compared to the high-dynamic pore pressures, and the pore pressures are equal to the wave pressure obtained from the wave model.

$$\sigma'_{sz} = \tau_s(x,0) = 0\,, \quad p_s = p_{wave} \tag{33}$$

Second, the bottom of the porous seabed with finite thickness h is considered as impermeable and rigid, so zero displacement and no vertical flow occur in the seabed bottom.

$$u_s = v_s = \frac{\partial p_s}{\partial z} = 0 \tag{34}$$

Third, the lateral boundary is considered impermeable and fixed horizontally, so the displacement on the x- direction and the gradient of pore pressure should all be zero.

$$u_s = \frac{\partial p_s}{\partial x} = 0 \tag{35}$$

2.4 Integration of wave and seabed models

In the integrated/coupled model, the wave motion and the porous flow is governed by the RANS equations, in which all the fluid properties, such as the continuity of pressure, velocity/flux of fluid are defined at the cell centroids. The least square linear reconstruction (LSLR) method of Bath (1992) is adopted to convert cell centroid data to face centroids for the evaluation of the quantity gradient at cell centroid. Time derivative is discretized by the forward time difference method. Based on Biot's dynamic (consolidation) poro-elastic theory, the seabed model was developed within COMSOL environment. In the coupling computation, only the wave pressure continuity is applied through the data exchange interface into the seabed surface to calculate the dynamic response of seabed around marine structure, including the displacements, pore pressure and the effective stresses.

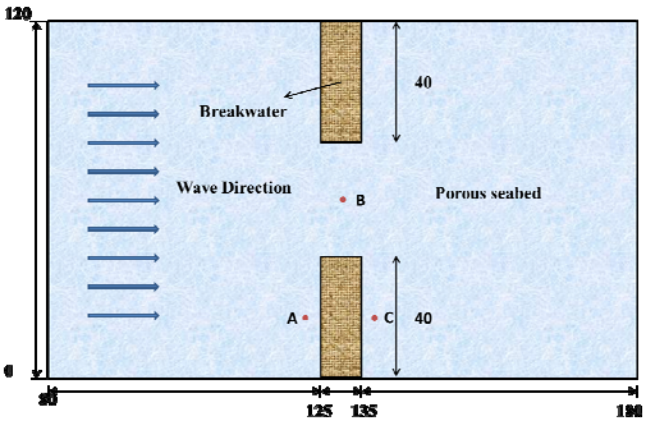

Fig. 1 Definition of wave-seabed interactions in the vicinity of breakwater heads

Table 1 Input data for parametric study

Seabed thickness (s)	5 m
Seabed length (l)	100 m
Poisson ratio (μ_s)	0.3
Soil porosity (n)	0.4
Shear modulus (G)	10^7 N/m^2
Permeability (K)	0.01 m/s or various
Degree of saturation (S_r)	0.975 or various
Wave period(T)	4sec or various
Wave height (H)	0.15 m
Water depth (h_w)	2 m

3. Results and discussions

The aim of this study is to examine the influence of wave-induced pore pressure in the vicinity of the breakwater. The effects of wave, seabed characteristics and breakwater configuration on soil response around the breakwater will be discussed through a set of parametric analysis. In this section, three representative locations around breakwater heads are selected, as shown in Fig. 1. Among these, Point A is located at the breakwater head, Point B is at the mid-point between two breakwater heads, and point C is beneath the breakwater. The input data for parametric study are given in Table 1.

3.1 Wave-induced pore pressure in the vicinity of the breakwater

The major difference between the present model and previous models for the wave-induced soil response around a marine infrastructure is the 3D effects around the structure. In this section, we further consider dynamic soil behavior in the present 3D porous model for wave-seabed-breakwater interaction problems. Figs. 2 and 3 illustrate the effects of fully-dynamic soil behaviour on the distributions of wave-induced pore pressure for various time intervals with two different wave periods. As seen in the figures, the magnitudes of the pore pressures beneath the breakwater are lower than that in front of a breakwater, and a longer wave period will cause large magnitude of pore pressure in the seabed. Figs. 2(c) and 3(c) clearly indicate that the influence of dynamic soil behavior is significant for the wave-induced pore pressure for both cases, especially for the locations in front of a breakwater. This is because the strong non-linear interactions between the incident waves, reflected waves and diffracted waves transfers faster than that in other area. This further enhances the acceleration due to solid and pore fluid. It was also found that, in the case of a wave period of 6 s, the differences are clearly shown between fully-dynamic and quasi-static solutions.

3.2 Effects of wave characteristics

Wave period is an important wave parameter, which directly affect the wavelength and other wave characteristics. In this section, we further investigate the effects of wave characteristics on

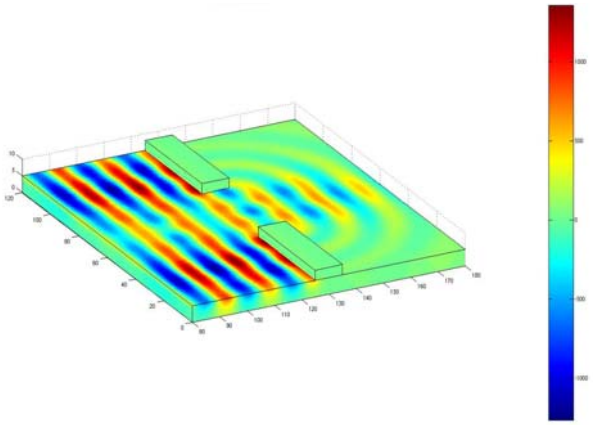

(a) $t / T = 0.25$

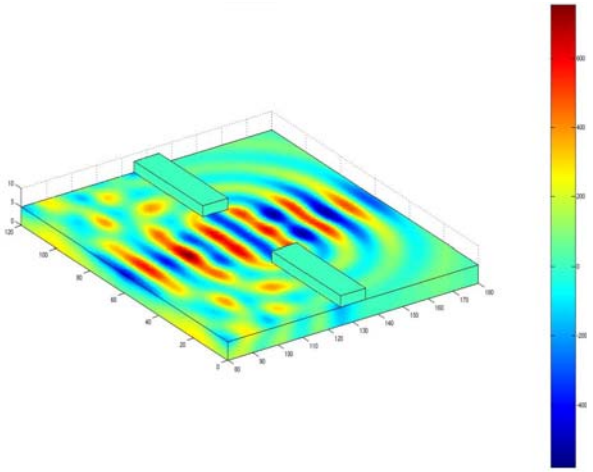

(b) $t / T = 0.5$

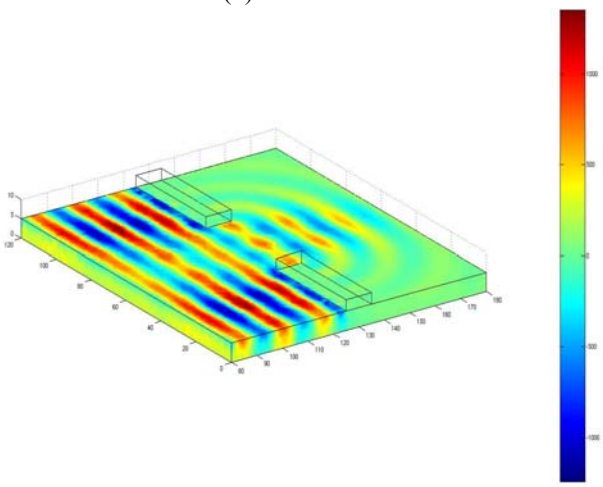

(c) $t / T = 0.75$

Fig. 2 Distributions of wave-induced pore pressure around breakwater heads for wave period of $T = 4$ sec

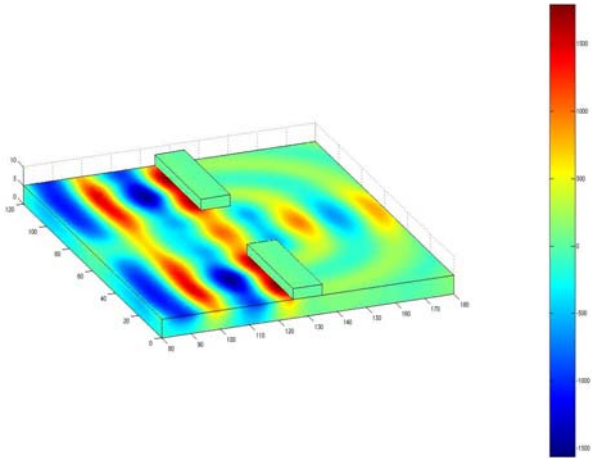

(a) $t / T = 0.25$

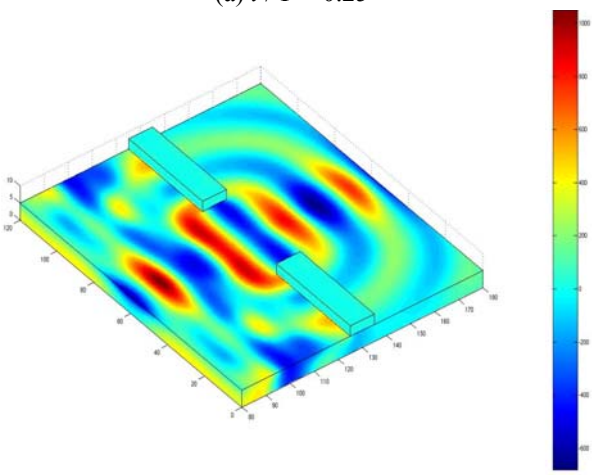

(b) $t / T = 0.5$

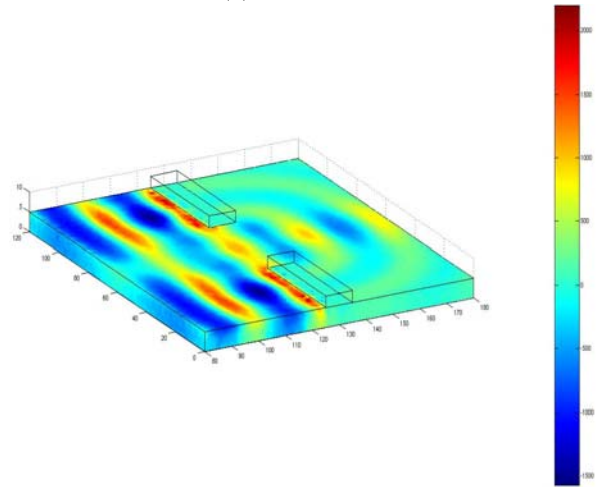

(c) $t / T = 0.75$

Fig. 3 Distributions of wave-induced pore pressure around breakwater heads for wave period of $T = 6$ sec

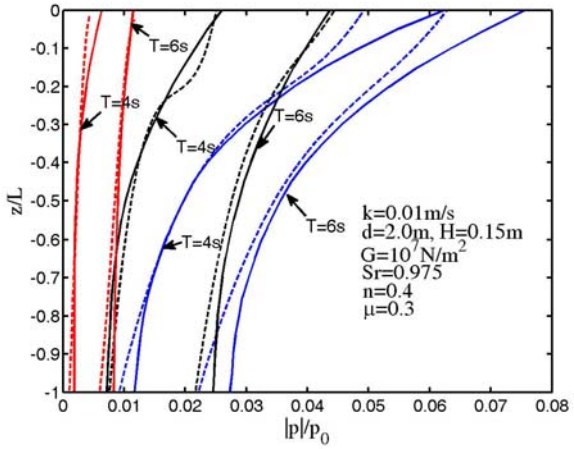

Fig. 4 Vertical distributions of wave-induced pore pressure versus the soil depth for various values of wave period (T) at three different locations (A = blue lines; B = black lines; C = red lines) around the breakwater head. Solid lines are quasi-static solutions, dashed lines are dynamic solutions

the wave-induced pore pressure around breakwaters at three different locations. The vertical distributions of maximum wave-induced pore pressure ($|p|/p_0$, where $p_0 = \gamma_w d$ is the static water pressure) in the vicinity of a breakwater for various values of wave period with different soil models (fully-dynamic and quasi-static) will be examined.

Fig. 4 illustrates the comparison of dynamic and quasi-static solutions on the wave-induced pore pressures $|p|/p_0$ at three different locations. As shown in the figure, the influence of wave period on the relative difference of wave-induced pore pressure between dynamic and quasi-static is more significant at location A than that at the other locations (B and C). This may be due to the faster loading caused by the wave reflection around the breakwater head. For both the two cases T = 4 s and T = 6 s, the pore pressure behind the breakwater is very small. In general, smaller wave period leads to a larger relative depth (d/L) when the water depth is assumed as a constant. This is the reason why a longer wave period will cause large magnitude of pore pressure in the seabed.

3.3 Effects of seabed characteristics

Besides the wave characteristics, soil property is another factor in the evaluations of wave-induced pore pressures in marine sediments. In this section, the effect of two important soil characteristics including the soil permeability and the degree of saturation on the wave-induced soil response will be investigated.

It was reported that, the compressibility of pore water is mainly dependent on the degree of saturation which plays an important role in the evaluation of the wave-induced seabed response (Okusa 1985, Hsu and Jeng 1994, Jeng 2013). In this study, three representative values of degree of saturation are chosen to investigate the wave-induced seabed response, and they are 95%, 97.5% and 99.5%, respectively. The vertical distributions of wave-induced pore pressure in coarse sands at three different locations with various degrees of saturation are illustrated in Fig. 5. As shown in Fig. 5, as the seabed saturation increases, the pore pressure increases in the seabed. The distribution of pore pressure changes smoothly at point C while it changes dramatically at the

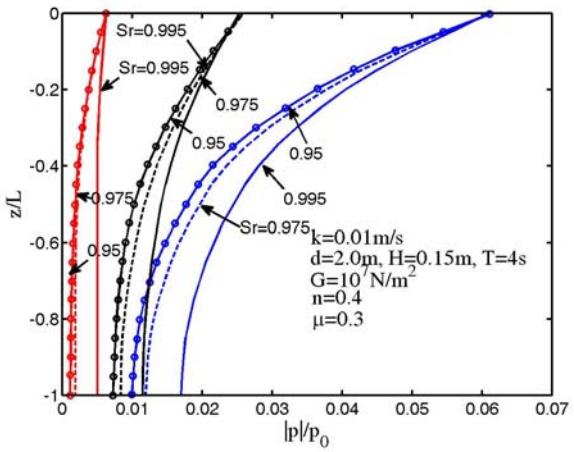

Fig. 5 Vertical distributions of wave-induced pore pressure versus the soil depth for various values of degree of saturation (S_r) at three different locations (A = blue lines; B = black lines; C = red lines) around the breakwater head

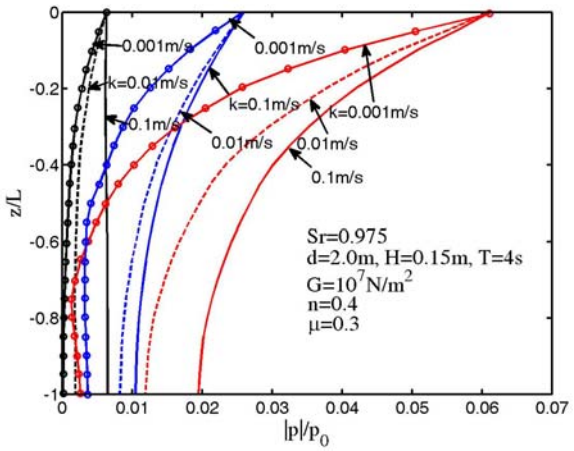

Fig. 6 Vertical distributions of wave-induced pore pressure versus the soil depth for various values of soil permeability (k) at three different locations (A = blue lines; B = black lines; C = red lines) around the breakwater head

others near the seabed surface. This should be attributed to the region where liquefaction may occur.

In addition to the degree of saturation, soil permeability is another important factor in the analysis of wave-induced soil response. Fig. 6 represents the vertical distributions of the relative difference of pore pressure versus soil depth in coarse and fine sand at three different locations. As shown in the figure, the pore pressures are higher at point A compared to those at point B and point C, where the pore pressures are obstructed by the breakwater. It was also found that, the pore pressure variation with relative soil depth at breakwater heads increases gradually in coarse sand, while they change rapidly near the surface of the seabed in fine sand. For the seabed beneath a breakwater, the pore pressure changes smoothly in both coarse sand and fine sand. Similar to the

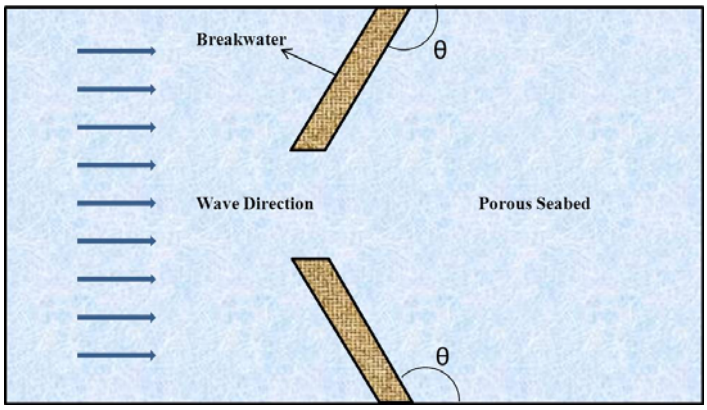

(a)

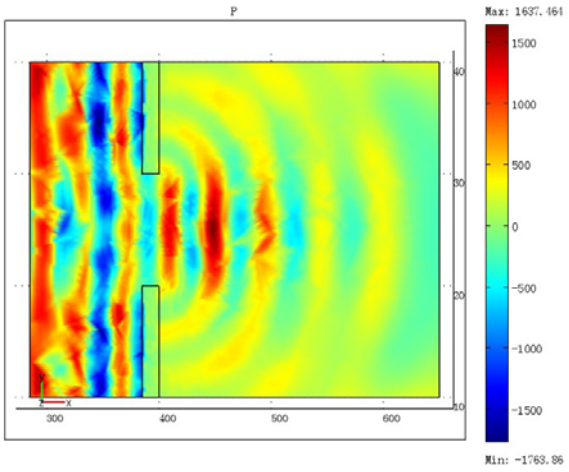

(b) $\theta = 90$

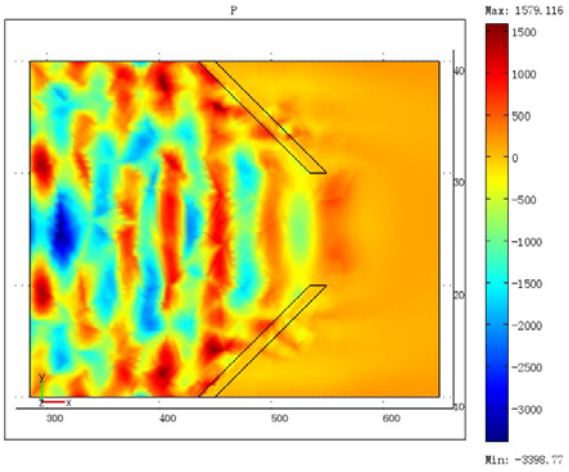

(c) $\theta = 30$

Fig. 7 Distributions of wave-induced pore pressure around breakwivter heads with different configuration of breakwaters

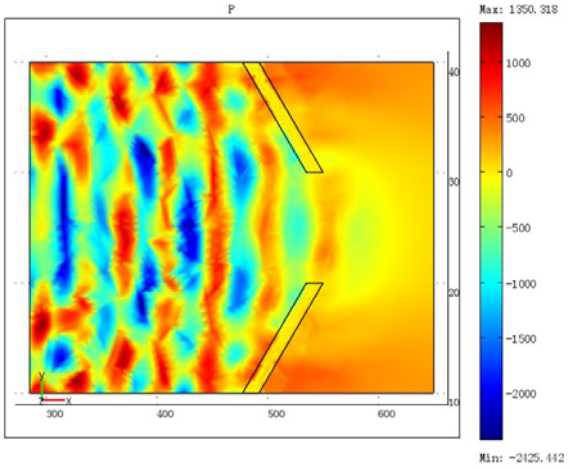

(d) $\theta = 45$

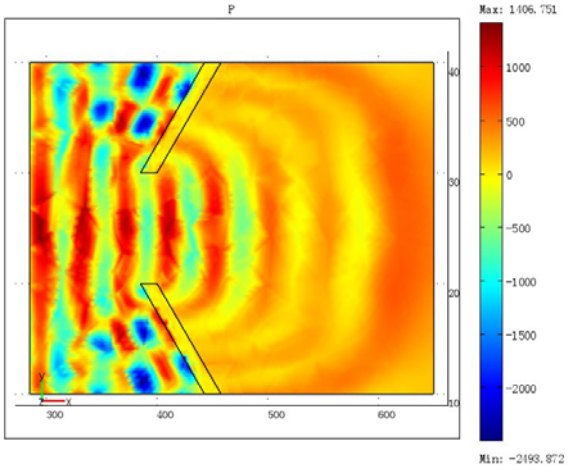

(e) $\theta = 120$

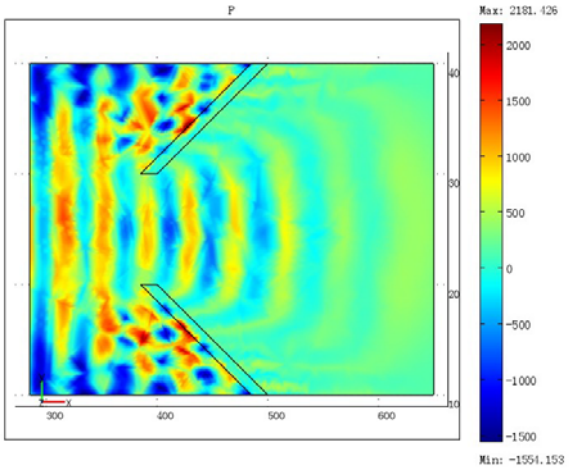

(f) $\theta = 135$

Fig. 7 Continued

Table 2 Input data for the cases with different breakwater configurations

Wave period (T)	5.0 sec or various
Water depth (d)	15.0 m or various
Wave height (H)	3.0 m or various
Seabed thickness (h)	20.0 m or various
Permeability ($_K$)	0.01 m/s or various
Degree of saturation (S)	0.98 or various
Soil porosity (n_s)	0.3
Poisson's ratio (μ_s)	0.4
Shear modulus (G)	10^7 N/m^2
Breakwater angle (θ)	90 degree or various

cases with various degree of saturation, soil permeability have great influence on the pore pressure at breakwater heads, but less for that beneath a breakwater.

3.4 Effects of breakwater configurations

Another new feature of this study is the effects of breakwater configurations, which cannot be examined in previous 2D models. Fig. 7 illustrates the contours of the pore pressures around breakwaters with different configurations at the depth 2 m below the seabed surface. The input data for these numerical examples are tabulated in Table 2. As shown in the figure, it can be seen that the patterns of pore pressure distributions are quite different with different configurations of breakwaters. Apart from this phenomenon, there is an overall upward trend of the pore pressures at the depth of 2 m beneath the seabed when the breakwater angles increase. This is due to the fact that larger angle of the breakwater induce more complicated interactions between the wave and the structure, and then further lead to the enormous differences among various configurations of the breakwater. This finding provides considerable evidence to the design and construction of the marine structures.

4. Conclusions

In this paper, we proposed a new 3D integrated model for the wave-induced pore pressure in a porous seabed around the breakwater heads. In this model, we integrate both wave and seabed models through the continuity of pressure along the seabed surface. Based on the numerical examples presented, the following conclusions can be drawn:

(1) The wave-induced pore pressure increases as the seabed permeability and degree of saturation increase.
(2) For the wave characteristics, the magnitude of wave-induced pore pressure is greater under the condition of a longer wave period.
(3) The configuration of breakwaters has a significant effect on the distribution pattern of pore pressure, and there is an overall upward trend of the pore pressures when the breakwater angles increase.
(4) The influence of fully-dynamic and quasi-static solutions on the wave-induced pore

pressure is more significant at location A than those at the other locations (B and C).

(5) The wave and soil characteristics have great influence on the pore pressure at breakwater heads, but less for that beneath a breakwater.

(6) In all cases, the wave-induced maximum pore pressure versus soil depth is much lower at location C (behind the breakwater) than those at other locations.

Acknowledgments

The authors are grateful for the support from Hohai University State Key laboratory of Hydrology-Water Resources and Hydraulic Engineering Open Fund Scheme.

References

Bath, T.J. (1992), Aspects of Unstructured Grids and Finite-Volume Solvers for the Euler and Navier-Stokes Equations", *AGARD*, Special Course on Unstructured Grid Methods for Advection Dominated Flows.

Biot, M.A. (1941), "General theory of three-dimensional consolidation", *J. Appl. Phys.*, **26**(2), 155-164.

Biot, M.A. (1956), "Theory of propagation of elastic waves in a fluid saturated porous solid, part I: Low frequency range", *J. Acoust. Soc.*, American, **28**(2), 168-180.

Gökee, T., Sumer B.M. and Fredsøe, J. (1994), "Scour around the head of a vertical-wall breakwater", *International Conference on Hydro-Technical Engineering for Port and Harbor Construction*, Yokosuka, Japan, 1097-1116.

Hsu, J.R.C. and Jeng, D.-S. (1994), "Wave-induced soil response in an unsaturated anisotropic seabed of finite thickness", *Int. J. Numer. Anal. Method. Geomech.*, **18**(11), 785-807.

Jeng, D.-S. (2003), "Wave-induced seabed instability in front of a breakwater", *Ocean Eng.*, **24**(10), 887-917.

Jeng, D.-S. (2013), *Porous Models for Wave-seabed Interactions*, Springer Berlin Heidelberg.

Jeng, D.-S. and Ou, J. (2010), "3D models for wave-induced pore pressure near breakwater heads", *Acta Mechanica*, **215**(1-4), 85-104.

Jeng, D.-S. and Seymour, B.R. (1997), "Response in seabed of finite depth with variable permeability", *J. Geotech. Geoenviron. Eng., ASCE*, **123**(10), 902-911.

Jeng, D.-S., Cha, D.H., Lin, Y.S. and Hu, P.S. (2000), "Analysis on pore pressure in a porous seabed in the vicinity of a caisson", *Applied Ocean Research*, **22**(6), 317-329.

Li, J. and Jeng, D.-S. (2008), "Response of a porous seabed around breakwater heads", *Ocean Eng.*, **35**(8-9), 864-886.

Lin, P. and Liu, P.L.-F. (1999), "Internal wave-maker for navier-stokes equations models", *J. Water. Port C.*, ASCE, **125**(4), 207-415.

Mase, H., Sakai, T. and Sakamoto, M. (1994), "Wave-induced porewater pressure and effective stresses around breakwater", *Ocean Engineering*, **21**(4), 361-379.

Norimi, M., Ayman, M.M. and Koichiro, I. (1998), "Nonlinear regular wave, submerged breakwater and seabed dynamic interaction", *Coast. Eng.*, **33**(2-3), 177-202.

Okusa, S. (1985), "Measurements of wave-induced pore pressure in submarine sediments under various marine conditions", *Mar. Geotechnol.*, **6**(2), 119-144.

Rodi, W. (1980), *Turbulence Models and their Application in Hydraulics State of the Art Review*, IAHR Publication.

Smith, A. and Gordon, A. (1983), "Large breakwater toe failures", *J. Water. Port C. ASCE*, **109**(2), 253-255.

Sumer, B.M. and Fredsøe, J. (2002), *The Mechanics of Scour in the Marine Environment*, World Scientific, Singapore.

Ulker, M., Rahman, M.S. and Guddati, M.N. (2010), "Wave-induced dynamic response and instability of seabed around caisson breakwater", *Ocean Engineering*, **37**(17-18), 1522-1545.
Yamamoto, T. (1977), "Wave induced instability seabed", *Proceedings of A.S.C.E. Special Conference*, Coastal Sediments, **77**, 898-913.
Zienkiewicz, O.C. and Shiomi, T. (1984), "Dynamic behavior of saturated porous media; the generalized biot formulation and its numerical solution", *Int. J. Numer. Anal. Method. Geomech.*, **8**(1), 71-96.

CC